catalysts

MDPI

Article

Cobalt Molybdenum Telluride as an Efficient Trifunctional Electrocatalyst for Seawater Splitting

Rajarshi Kar, Amideddin Nouralishahi, Harish Singh and Manashi Nath *

Department of Chemistry, Missouri University of Science and Technology, Rolla, MO 65409, USA
* Correspondence: nathm@mst.edu

Abstract: A mixed-metal ternary chalcogenide, cobalt molybdenum telluride (CMT), has been identified as an efficient tri-functional electrocatalyst for seawater splitting, leading to enhanced oxygen evolution reaction (OER), hydrogen evolution reaction (HER), and oxygen reduction reaction (ORR). The CMT was synthesized by a single step hydrothermal technique. Detailed electrochemical studies of the CMT-modified electrodes showed that CMT has a promising performance for OER in the simulated seawater solutions, exhibiting a small overpotential of 385 mV at 20 mA cm^{-2}, and superior catalyst durability for prolonged period of continuous oxygen evolution. Interestingly, while gas chromatography analysis confirmed the evolution of oxygen in an anodic chamber, it showed that there was no chlorine evolution from these electrodes in alkaline seawater, highlighting the novelty of this catalyst. CMT also displayed remarkable ORR activity in simulated seawater as indicated by its four-electron reduction pathway forming water as the dominant product. One of the primary challenges of seawater splitting is chlorine evolution from the oxidation of dissolved chloride salts. The CMT catalyst successfully and significantly lowers the water oxidation potential, thereby separating the chloride and water oxidation potentials by a larger margin. These results suggest that CMT can function as a highly active tri-functional electrocatalyst with significant stability, making it suitable for clean energy generation and environmental applications using seawater.

Keywords: seawater splitting; oxygen evolution reaction; oxygen reduction reaction; hydrogen evolution reaction; tri-functional electrocatalyst

Citation: Kar, R.; Nouralishahi, A.; Singh, H.; Nath, M. Cobalt Molybdenum Telluride as an Efficient Trifunctional Electrocatalyst for Seawater Splitting. *Catalysts* **2024**, *14*, 684. https://doi.org/10.3390/catal14100684

Academic Editors: Yurii V. Geletii and Tam D. Nguyen

Received: 31 August 2024
Revised: 24 September 2024
Accepted: 27 September 2024
Published: 2 October 2024

1. Introduction

While water electrolysis presents an attractive solution for green hydrogen generation, the dearth and unequal distribution of clean water across the globe creates a formidable challenge for the widespread adoption of this technology. Naturally occurring seawater, on the other hand, offers a sustainable and promising resource for the production and storage of green energy through three main electrochemical reactions, i.e., oxygen evolution reaction (OER), hydrogen evolution reaction (HER), and oxygen reduction reaction (ORR). It also supports global initiatives to reduce carbon emissions and shift towards renewable energy. Enhancing seawater splitting technology can lead to substantial economic, environmental, and technological advantages, fostering a greener and more sustainable future. However, like water splitting, a core challenge in electrocatalytic seawater splitting also lies with the choice of electrocatalysts. Designing effective electrocatalysts to split seawater is critical to achieve feasibility and minimize cost for large-scale hydrogen and oxygen production [1]. Moreover, the compositional complexity of catalysts for seawater splitting are more demanding compared to electrocatalysts used to split pure water due to the unfavorable chlorine chemistry, which causes catalyst poisoning [2]. Since OER, HER, and ORR are central to the development of efficient green hydrogen technologies, advances in catalysts and materials that facilitate these reactions, leading to sustainable, cost-effective, and high-performance energy systems, are desired to help transition to a cleaner and more sustainable energy future [3,4].

A key challenge in seawater electrolysis is suppressing chlorine evolution reaction (CER), which produces harmful chlorine gas both polluting the environment as well as suppressing OER. The adsorption of chloride ions (Cl^-) from salts present in seawater during OER tends to compete with the adsorption of hydroxyl (OH^-) ions which eventually impedes the reaction and leads to the formation of chlorine-containing products. Chloride ion adsorption further stimulates the degradation or corrosion of the electrocatalyst and their metal substrates and eventually blocks the active site on the catalyst [5]. The presence of chloride ions (Cl^-) in NaCl can also inhibit the hydrogen evolution reaction (HER) through various mechanisms such as catalyst poisoning, the alteration of the hydrogen binding energy, the corrosion or passivation of the catalyst through surface modification, a shift in the equilibrium potential, and an increase in overpotential. These effects must be considered in designing and optimizing electrochemical systems where HER plays a crucial role [6]. The high concentration of chloride ions (Cl^-) in seawater can also adversely affect the oxygen reduction reaction (ORR), leading to the corrosion of electrodes, destabilization of catalysts due to phase transitions in the catalyst material, and increased overpotential [7–10]. Additionally, in electrolytic seawater splitting, an increase in pH (pH > 9.5) is observed locally near the electrodes, which results in insoluble deposits of cations (e.g., Mg^{2+} and Ca^{2+}) on the electrode surface, thus blocking some active sites, which eventually leads to a reduction of catalytic performance in OER, HER, and ORR [11]. Therefore, designing an active, selective, and stable electrocatalyst which can also tackle complex seawater environments is in growing need [12–14].

An effective electrocatalyst with a reduced onset overpotential and improved energy efficiency plays a vital role in increasing the feasibility of large-scale water-splitting reactions. Thus, significant efforts have been targeted to design more efficient, robust, and stable OER catalysts which has the capability of reducing the overpotential. Most of the conventionally used state-of-the-art electrocatalysts for water splitting are those based on noble metals such as platinum (Pt), iridium (Ir), and ruthenium (Ru) [15], but they face some constraints when used for industrial usage due to their high cost, rarity, and unsatisfactory durability [16]. Hence, the substitution of noble metal electrocatalysts with a non-precious metal for catalyzing the OER and HER are of growing interest [17]. Recently, transition metal chalcogenides (TMC) have been identified as a high-efficiency, durable electrocatalyst for OER, thereby offering a promising solution to the limitations posed by the cost and scarcity of raw materials needed for synthesizing noble metal oxides like IrO_2 and RuO_2 [18]. The TMCs have attracted great attention due to their promising electrocatalytic activity toward OER, ORR, and HER supported by their amenable surface morphologies, high tunability of electronic structures, rich active sites, being economically favorable, and their ability to keep Cl^- ions away from the active material during electrolysis through electrostatic repulsion [19,20]. Moreover, TMCs, which range from semiconductors to semimetallics typically exhibit much higher electrical conductivity than transition metal oxides (TMOs), which are mostly insulating. This enhanced electrocatalytic activity is attributed to the decrease in the electronegativity of the chalcogen atom within the TMC series, leading to heightened covalency in the metal–chalcogen bonds, and improved electrochemical activity of the transition metal center. The increased covalency also leads to an enhanced charge transfer. Transition metal chalcogenides (TMCs) can also be doped to fine-tune the electronic structure of individual metal sites in multinary transition metal-based electrocatalysts, offering new avenues for enhancing oxygen evolution reaction (OER) performance across a broad spectrum of systems [21,22]. Moreover, TMCs, owing to their ability to adopt various oxidation states for the transition metal center, facilitate and enhance redox reactions, further bolstering their efficacy as electrocatalysts [23]. Additionally, TMCs exhibit chemical stability in acidic and alkaline media, which makes it corrosion-resistant, and have superior robustness [24,25].

In this current study, a mixed-metal chalcogenide, cobalt molybdenum telluride (CMT), has been examined as a novel tri-functional electrocatalyst for HER, OER, and ORR reactions in simulated seawater. The CMT samples have been synthesized through a

simple one-step hydrothermal procedure, and their electrochemical performance has been studied through a variety of electrochemical techniques. It was observed that while cobalt molybdenum telluride (CMT) could effectively produce hydrogen and oxygen through seawater splitting at relatively low overpotentials, it did not lead to any chlorine evolution. Thereby, CMT can be considered a promising electrocatalyst for clean energy applications with a remarkable performance in naturally occurring seawater. The CMT composite electrocatalyst for seawater splitting has been reported for the first time. Although transition metal chalcogenides have been reported for water splitting, there has been very few reports on seawater splitting with a high salt concentration. Moreover, this catalyst is also active for HER and ORR in seawater, increasing the novelty. Hence, this study provides a route for generating hydrogen energy from abundant saltwater sources instead of freshwater. The process not only aims to meet the growing global energy demand but also addresses crucial sustainability concerns related to freshwater resource scarcity and environmental impact.

2. Results and Discussion

2.1. Structural and Morphological Characterization

Powder X-ray diffraction (PXRD) patterns were used to corroborate the phase purity and crystallinity of the synthesized CMT electrocatalyst. Figure 1a shows the PXRD patterns of hydrothermally synthesized cobalt molybdenum tellurides (CMT) along with the standard patterns of CoTe and $MoTe_2$ as reported in powder diffraction database, PDF# 00-034-0420 and PDF# 00-73-1650, respectively. As shown in Figure 1a, the PXRD pattern of the CMT electrocatalyst contains the main peaks of the CoTe and $MoTe_2$ phases. This suggests that CMT yielded a mixture of CoTe and $MoTe_2$ phases, showing a successful synthesis of cobalt molybdenum telluride, henceforth referred to as CoMoTe. Some diffraction peaks corresponding to lattice planes of $CoTe_2$ were also observed near 28° and 48° (<1 1 0> and <1 0 3>, respectively), which indicates that there might be a trace amount of $CoTe_2$ present in the CoMoTe sample [26]. The morphology of the CoMoTe sample was investigated thorough SEM micrograph, as shown in Figure 1b. The as-synthesized pristine CoMoTe sample showed sparsely populated dense floret-like octahedral clusters with rough edges and an estimated average size of 20–30 nm.

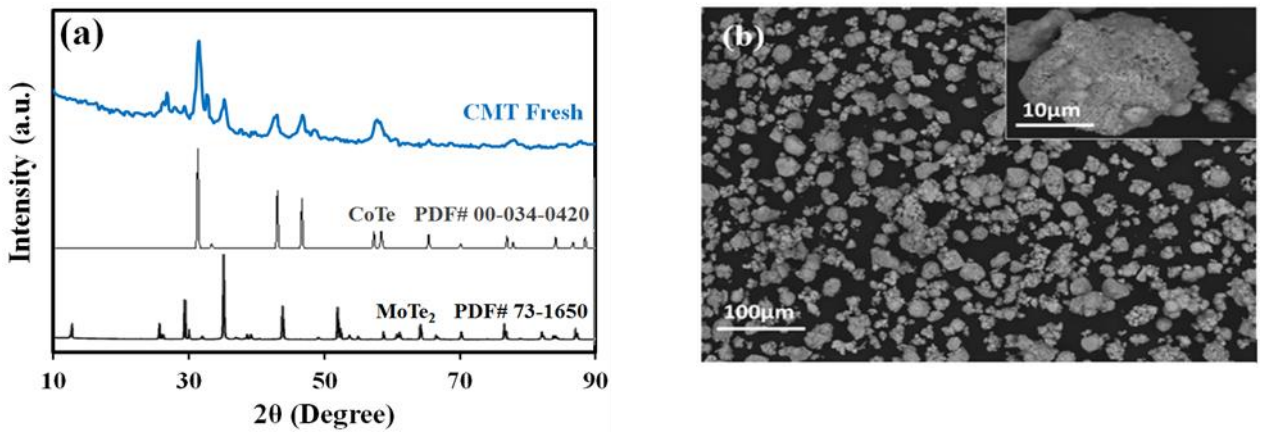

Figure 1. (**a**) PXRD patterns of CMT; (**b**) SEM images of CMT.

The composition of the CoMoTe catalyst was studied through high-resolution XPS spectra, as shown in Figure 2. The three peaks centered at 230.0 eV, 232.4 eV, and 235.3 eV, as shown in Figure 2a, corresponds to Mo^{4+} and Mo^{6+}, respectively [27]. The XPS spectra for Te (Figure 2b) show peaks at a binding energy of 576.5 and 586.8 eV, which corresponds to Te $3d^{5/2}$ and Te $3d^{3/2}$, correlating well with the presence of Te^{2-} [28]. In Figure 2c, Co2p XPS spectra exhibits two peaks at 780.15 and 797.25 eV, corresponding to $2p^{3/2}$ and $2p^{1/2}$, respectively, which correspond to the presence of Co^{2+} [29,30]. The satellite peaks for Co^{2+} were also observed at 786.8 and 803.5 eV, as reported in the literature [31]. The

XPS spectra were also used for quantitative analysis of electrode surface for the CoMoTe catalyst, and the results are listed in Table 1. It was observed that the relative atomic ratio of Mo:Co:Te was close to 1:1:3, which further confirmed the presence of $MoTe_2$ and CoTe in the composite.

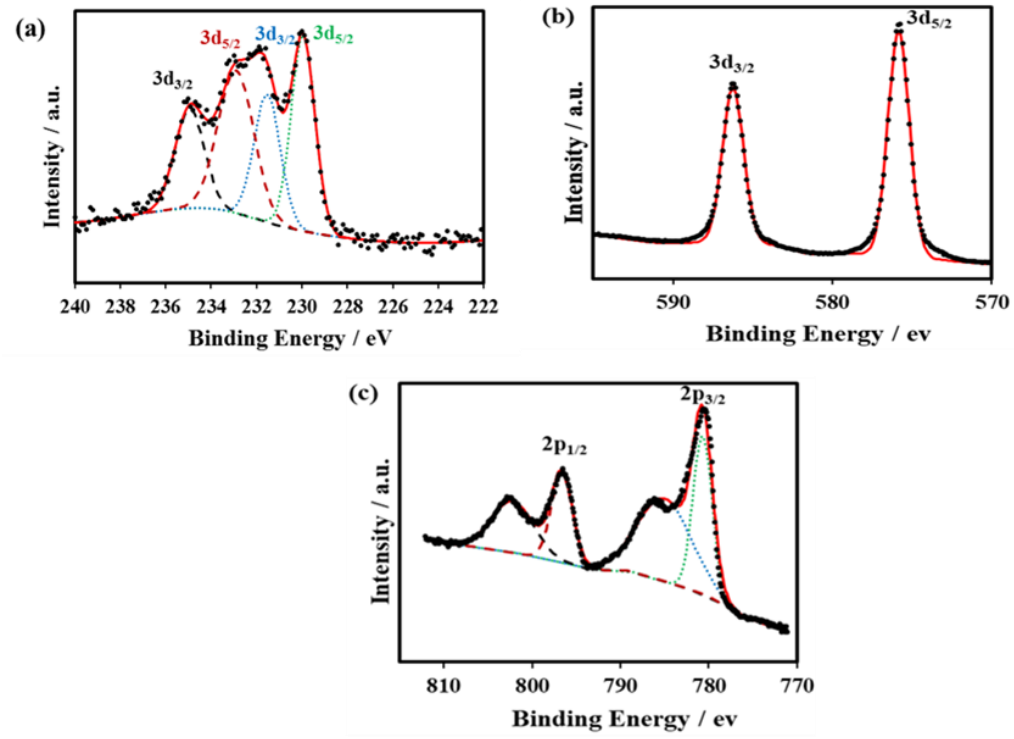

Figure 2. The deconvoluted XPS spectra of CMT electrocatalyst: (**a**) Mo 3d, (**b**) Te 3d, (**c**) Co 2p peaks.

Table 1. Quantitative analysis of XPS for CMT for before after the reaction.

Elements	As Prepared CMT At%	Used CMT At%
Mo	19.01	19.02
Co	19.33	20.76
Te	55.93	52.10
O	5.73	8.13

2.2. Electrocatalytic Performance of CoMoTe in OER

The electrocatalytic activity of CoMoTe for OER reaction at different concentrations of NaCl has been examined by linear sweep voltammetry experiment as shown in Figure 3a. An overpotential of 340 mV was obtained at 20 $mAcm^{-2}$ in 1M KOH, which is superior to that reported for state-of-the-art RuO_2 catalyst which exhibits an overpotential of about 397 mV under similar experimental conditions, [32] suggesting the high performance of CoMoTe electrocatalyst in OER. Besides the low overpotential, CoMoTe also showed high current density in all the electrolyte solutions which demonstrates facilitated charge transfer on the electrocatalyst surface, further elucidating its superior catalytic activity. The onset potential of OER on CoMoTe increases with higher NaCl concentrations, which is in good accordance with previous reports on the effect of salt concentration [32]. As the salt concentration in the electrolyte was varied, the overpotential at 20 $mAcm^{-2}$ increased from 340 mV in 1 M KOH to 385 mV and 400 mV, respectively, in the 1 M KOH + 0.1 M NaCl, and 1 M KOH + 0.3 M NaCl electrolytes. These data suggest that at higher salt concentrations, there might be some surface passivation with chloride adsorption leading to the requirement of a higher voltage for water oxidation [33,34].

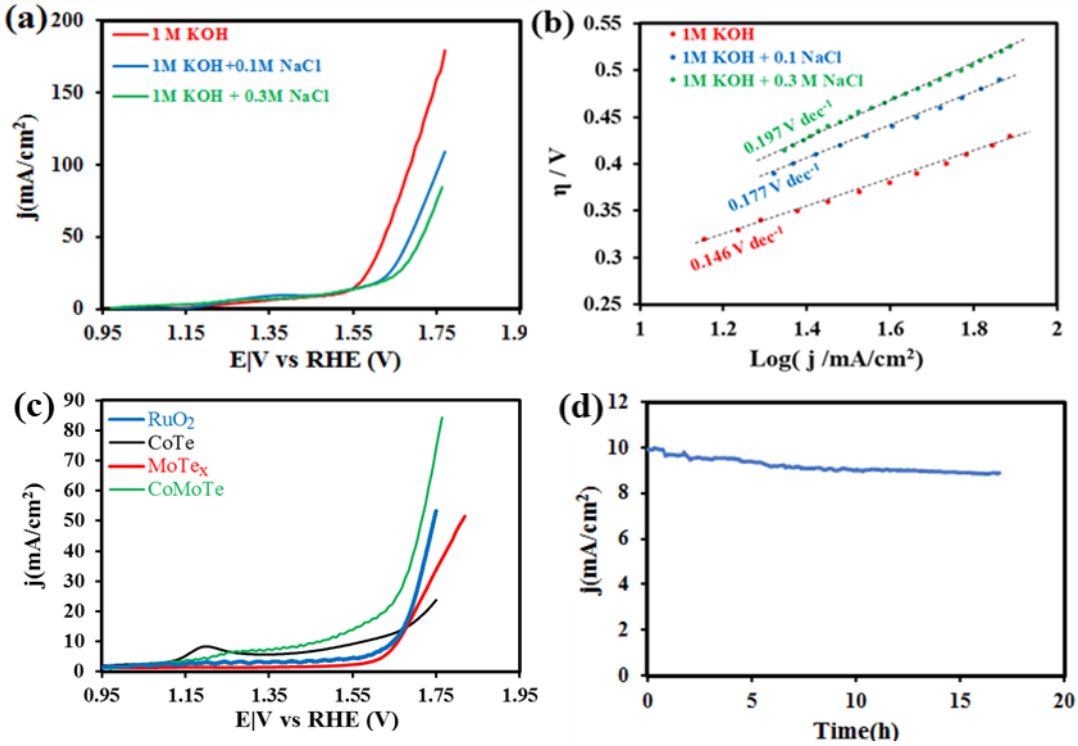

Figure 3. (**a**) LSV plots of the as-prepared CMT at different salt concentration (measured with a scan rate of 10 mV s^{-1}). (**b**) The Tafel plots of CMT at different salt concentration. (**c**) Comparative LSV results at 1 M KOH + 0.3 M NaCl. (**d**) Chronoamperometry test of CMT at a 600 mV of applied potential.

The Tafel slope is a critical parameter to study the mechanism of electrocatalytic reactions and extract kinetic information, such as the rate-determining step in the OER. A small Tafel slope indicates faster reaction kinetics, thereby, higher electrochemical activity [35,36]. The Tafel slopes of CoMoTe estimated in 1 M KOH, 1 M KOH + 0.1 M NaCl, and 1 M KOH + 0.3 M NaCl electrolytes were 146 mV dec^{-1}, 177 mV dec^{-1}, 197 mV dec^{-1}, respectively, which corroborates well with the linear scan voltammogram data and confirms the slight inhibition of OER kinetics in the presence of high salt concentration. Nevertheless, the low overpotential and high current density of CoMoTe illustrates the superior performance of this electrocatalyst for seawater splitting. The OER catalytic activity of CoMoTe was also compared with that of the binary tellurides, CoTe and $MoTe_2$, as well as RuO_2, as shown in Figure 3c. It was observed that the CoMoTe shows lower overpotential as well as produces superior current density at the highest salt concentration of 1 M KOH + 0.3 M NaCl, in comparison to the binary tellurides. This can be attributed to the scrambling of the catalytic sites in CoMoTe leading to synergistic effects, which promotes catalyst site activation and further electrocatalytic property. The CoMoTe catalyst also showed enhanced activity both in terms of lower overpotential and higher current density than state-of-the-art RuO_2 in alkaline seawater.

The catalyst stability for extended period of seawater splitting was studied through constant potential chronoamperometry. Figure 3d shows the chronoamperometry results at a constant applied potential of 0.6 V vs Ag | AgCl for 18 h to evaluate the electrochemical stability of the CoMoTe in artificially simulated seawater (i.e., 1 M KOH + 0.3 M NaCl). From the chronoamperometry data, it was observed that after OER for over 18 h, CoMoTe was still capable of retaining 89% of its initial current density, showing that this electrocatalyst exhibits excellent long-term functional stability for seawater splitting. The observed degradation of current density in long-term chronoamperometry may be explained by gradual leaching of the electrocatalyst layer owing to the continuous evolution of gaseous O_2. The continuously generated bubbles create a porous electrode surface which leads

to some loss of catalyst on long-term operation. The exceptional OER performance in CMT showcases that despite the presence of chloride anions in seawater, which induce a competing chlorine evolution reaction, CoMoTe electrocatalyst maintained its functional activity and demonstrated an impressive current density for prolonged period of operation.

The compositional stability of CoMoTe after prolonged OER in seawater was studied through the SEM, PXRD, and XPS measured after 18 h chronoamperometry (Figure 4). SEM analysis showed no remarkable change in their average size or morphology of the catalyst grains, as shown in Figure 4a. This is in good agreement with the respective PXRD data shown in Figure 4b, where the peak patterns are similar to those reported for the fresh CoMoTe electrocatalyst. The XPS analysis showed Mo having peaks at 229.8, 232.98 eV, and 234.88 eV corresponding to Mo^{4+} and Mo^{6+}, respectively. Te has peaks at binding energy of 575.6 eV and 586 eV, which corresponds to Te $3d^{5/2}$ and Te $3d^{3/2}$, and Co has peaks at 780.1 eV and 795.7 eV, corresponding to $2p^{3/2}$ and $2p^{1/2}$, as shown in Figure 4c–e. Comparison of the XPS peaks before and after chronoamperometry showed that there are no significant peak shifts, and the XPS patterns were superimposable on each other. The quantitative analysis of the XPS peaks after chronoamperometry also showed a similar relative ration of Mo:Co:Te as obtained from the pristine sample, as shown in Table 1. Hence, the characterization data presented in Figure 4 support the exceptional stability of the CMT electrocatalyst during long-term operation in alkaline seawater. In our previous studies with selenide and telluride electrocatalysts, we have shown the extensive stability of these chalcogenides against compositional degradation. We have also shown that the dynamic reconstruction at the surface involves the formation of a mixed-anionic oxychalcogenide surface through catalyst site activation through hydroxyl attachment [32]. The current study with the CoMoTe electrocatalyst also shows a similar trend of surface and compositional stability that can expectedly arise from the facile catalyst site activation at lower overpotentials.

The gas products released during the oxygen evolution reaction with CoMoTe electrocatalyst have been analyzed by an gas chromatograph equipped with thermal conductivity detector (GC-TCD), and the results are presented in Figure 5. The collected headspace gas from the anodic chamber was analyzed along with the GC-TCD data obtained from the injection of standard gases, i.e., pure oxygen, nitrogen, and chlorine. The gas that evolved near the anode was collected over a 12 h period, and samples from this headspace gas were injected into the gas port of the GC-TCD. As observed in Figure 5, only the peaks corresponding to oxygen and nitrogen were present in the collected headspace gas, while no chlorine was detected. This confirms the selectivity of this catalyst towards water oxidation exclusively, even in the presence of high salt concentration. The GC-TCD study further confirms the immense potential of CoMoTe electrocatalyst for clean energy production from seawater with high salinity.

To further investigate the effect of variable NaCl concentration on the electrocatalytic performance of CoMoTe in the OER reaction, electrochemical impedance spectroscopy (EIS) was conducted. Figure 6 shows the EIS studies in 1 M KOH and 1 M KOH + 0.3 M NaCl electrolytes, while the inset shows a simple equivalent circuit model that has been used to fit the EIS data. Here, R_S represents the solution resistance, R_C represents the resistance of the corrosion layer formed at the electrode surface, R_{CT} stands for the charge transfer resistance at the electrolyte–electrode interface, and CPE1 and CPE2 are the constant phase elements [37]. The charge transfer resistance at the electrode–electrolyte interface (R_{CT}) for CoMoTe in 1 M KOH was estimated to be 8.193 Ω, while the R_{CT} for 1 M KOH + 0.3 M NaCl was estimated to be 20.49 Ω. The slight increase in the charge transfer resistance is probably due to the presence of chloride (Cl^-) ions in seawater which impedes the hydroxyl ion diffusion near the surface. However, the fact that there is no chlorine evolution illustrates the higher intrinsic catalytic activity of this electrocatalyst for OER in seawater despite the high salinity. The electrolyte resistance on the other hand stayed almost similar for 1 M KOH (9.139 Ω) and 1 M KOH + 0.3 M NaCl (8.538 Ω), indicating similar internal resistance of the electrolyte, thus confirming the observed difference

in activity is solely due to the intrinsic property of the catalyst composite and the variable electrode–electrolyte interface.

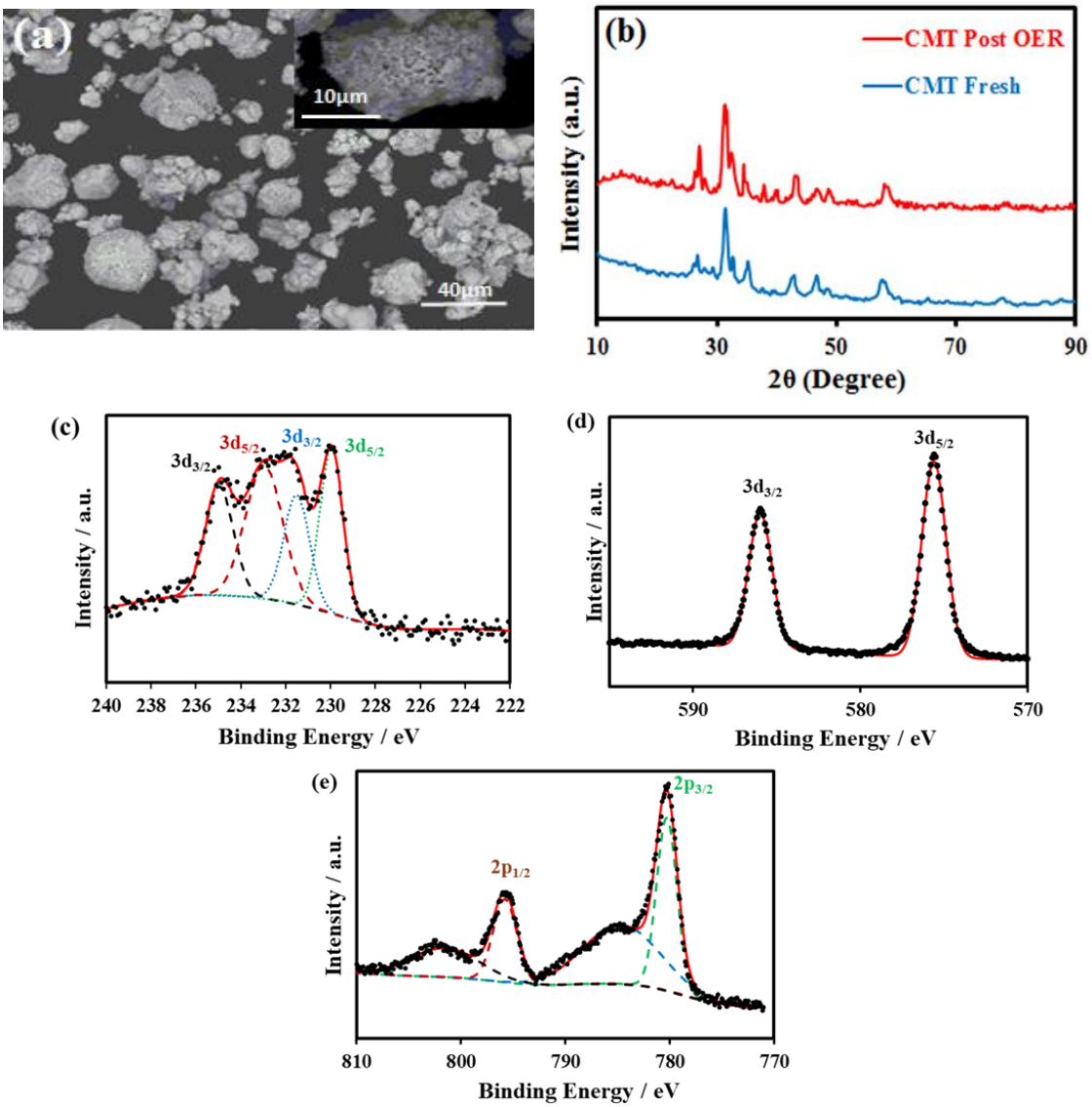

Figure 4. Post activity characterization data of CMT. (**a**) SEM images after chronoamperometry; (**b**) PXRD pattern before and after chronoamperometry; (**c**) XPS spectra of Mo; (**d**) XPS spectra of Te; (**e**) XPS spectra of Co.

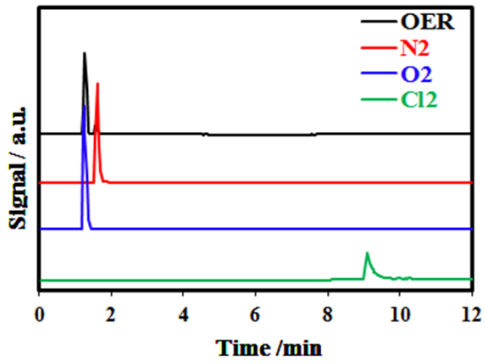

Figure 5. Chromatogram of gas products of OER on CMT electrocatalyst after chronoamperometry experiment at 600 mV for 17 h, as well as pure chlorine, oxygen, and nitrogen gases.

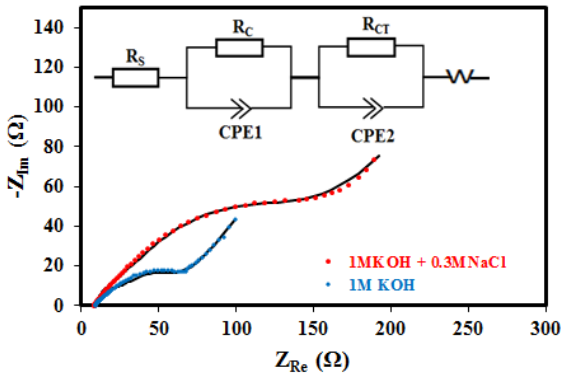

Figure 6. Electrochemical impedance spectra of CoMoTe electrocatalyst in 1 M KOH and 1 M KOH + 0.3 M NaCl electrolytes. The EIS data have been recorded at 400 mV (vs Ag | AgCl) in the frequency range of 0.1 Hz to 100 kHz.

2.3. Electrocatalytic Performance of CoMoTe for HER

The electrocatalytic activity of CMT in HER from seawater has been presented in Figure 7a, which shows the results of linear sweep voltammetry (LSV) in a 1 M KOH solution containing different amounts of NaCl. As is evident from the LSV data, the synthesized CoMoTe showed impressive HER catalytic activity in both NaCl concentrations exhibiting an overpotential of 280 mV in 1 M KOH, 350 mV in 1 M KOH + 0.1 M NaCl, 455 mV in 1 M KOH+ 0.3 M NaCl at the current density of 10 mA cm^{-2}, as shown in Figure 7a. The increasing overpotential for HER in the presence of higher NaCl concentration can be attributed to the presence of excess chloride ions in the vicinity of the catalyst surface, which inhibits formation of the surface charge layer for HER. The chloride ions restrict the charge transfer between the electrolyte and the electrode, which weakens HER activity [38]. The competition from the chloride ion adsorption requires additional energy to maintain the desired rate of HER, thus increasing the overpotential. Additionally, increased concentrations of cations like sodium (Na^+) can compete with hydrogen ions (H^+) for adsorption sites on the electrode surface [39]. This competition can also reduce the availability of active sites for HER, leading to higher overpotentials.

The catalyst stability under the condition of continuous hydrogen evolution in seawater has been analyzed through chronoamperometry experiment at a constant applied potential of −500 mV vs Ag | AgCl, as shown in Figure 7b. As can be observed, CoMoTe electrocatalyst maintained its activity for HER reaction during a prolonged operational time period of 20 h, which suggests that the electrocatalyst did not experience significant degradation or loss of hydrogen evolution ability. This further demonstrates that the material is both active and corrosion-resistant in a chloride-rich environment [40]. The high stability of CoMoTe in HER reaction may be attributed to its resistance against catalyst poisoning, resistance against corrosion, and its inertness toward reduction of anions [41].

Since CoMoTe was found to be efficiently active both for OER and HER in saline water, a full seawater electrolysis cell was assembled by employing CoMoTe on both the cathode and the anode electrodes in alkaline water with a 0.1 M NaCl concentration and the results are presented in Figure 7c. On conducting full water electrolysis, it was observed that CoMoTe could effectively split water and yield a current density of 10 mA cm^{-2} at a cell voltage of 1.59 V in artificial seawater electrolyte comprising 1 M KOH + 0.1 M NaCl. The remarkable HER performance of CoMoTe electrocatalyst exhibits that, at high salt concentrations in seawater, even though the HER can be more competitive due to the suppressing chlorine evolution reaction (CER), hydrogen production was still favored over CER products. The high stability of CoMoTe for HER in seawater also shows that this electrocatalyst surface is resistant to degradation by chloride ions, suggesting CoMoTe as a promising electrocatalyst for seawater electrolysis.

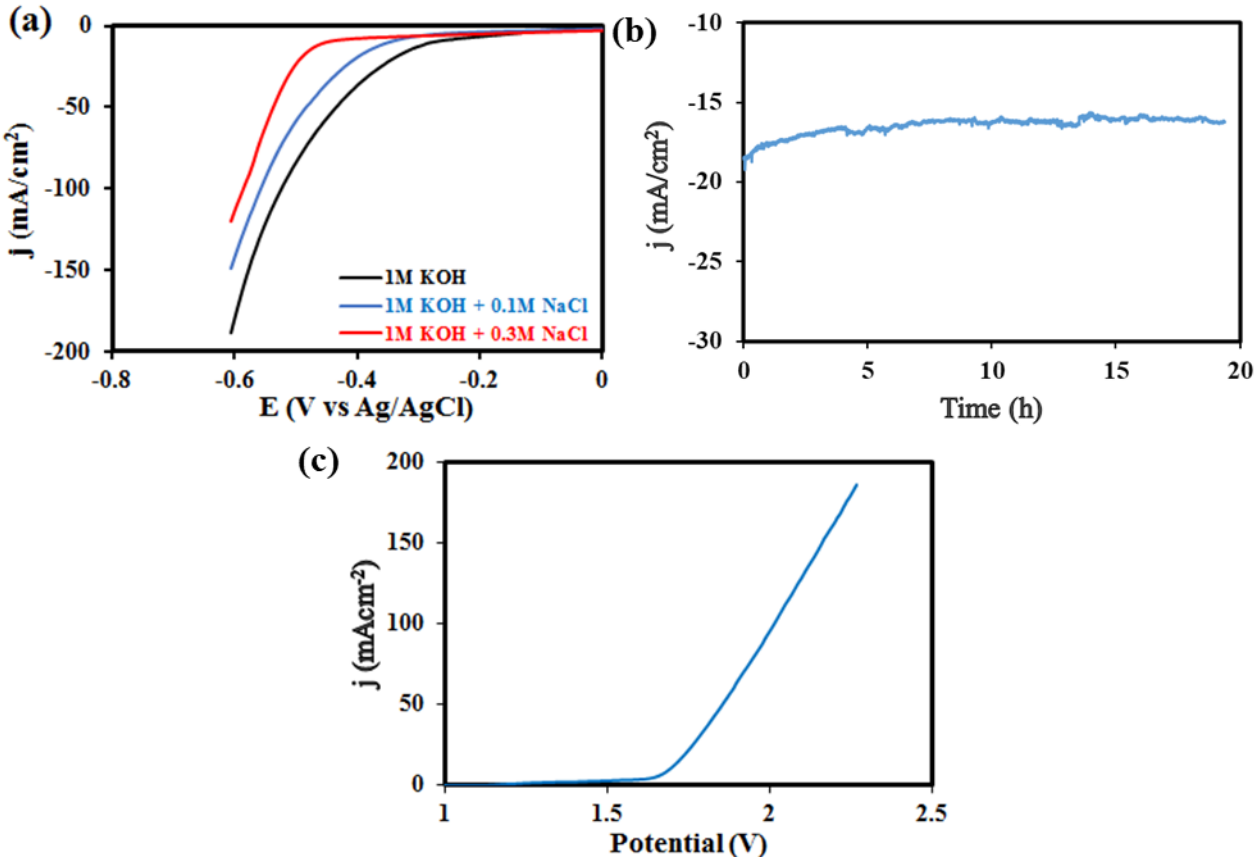

Figure 7. (**a**) LSV plots of HER reaction CMT at different NaCl concentrations at scan rate of 10 mV s^{-1}. (**b**) Chronoamperometry plots illustrating long-term stability of CMT electrode under −500 mV of applied potential. (**c**) LSV curve of the full water electrolysis on CMT.

2.4. Electrocatalytic Performance for ORR

The electrocatalytic performance of CoMoTe for ORR has been investigated by LSV in 1 M KOH, 1 M KOH + 0.3 M NaCl, and 1 M KOH + 0.1 M NaCl with rotating disk electrodes (RDE) set up at different rotation speeds (Figure 8a–c). From the polarization curves in Figure 8a–c, it can be deduced that the current density amplifies with the increasing rotation speed. This is compatible with the data reported in the literature and may be attributed to the accelerated diffusion within the electrolyte facilitating the reactant access to the active sites [42]. Figure 8d shows the bar plot of the reduction current density at 2000 RPM for the different types of electrolytes. It can be observed that in 1 M KOH, CoMoTe exhibits the highest diffusion limited current density at 2000 RPM followed by 1 M KOH + 0.1 M NaCl and 1 M KOH + 0.3 M NaCl. The decline in current density with the increasing salt concentration can be attributed to the influence of negatively charged chloride ions on the ORR, which can lower the ORR efficiency, leading to higher overpotentials and reduced current density for the same reaction rate [43,44].

The ORR onset potentials, half-wave potentials, and diffusion-limited current density in electrolytes with different concentrations of NaCl are shown in Table 2. While the onset potential for ORR remained similar under increasing salt concentration, indicating similar catalytic activity, the diffusion-limited current density showed a slight decrease, which can be due to the increased concentration of chloride ions in the vicinity of the surface, which leads to hindrance in diffusion and efficient adsorption of the oxygenated ionic species. Previous research has also shown that the salt ions, especially chloride ions, can adsorb onto the electrode surface and block active sites necessary for the ORR, reducing the effective surface area for the reaction and thereby decreasing the reduction current

density [45]. In addition, the lower diffusion-limited current density might also be due to the higher viscosity and lower oxygen dissolution of artificial seawater [46].

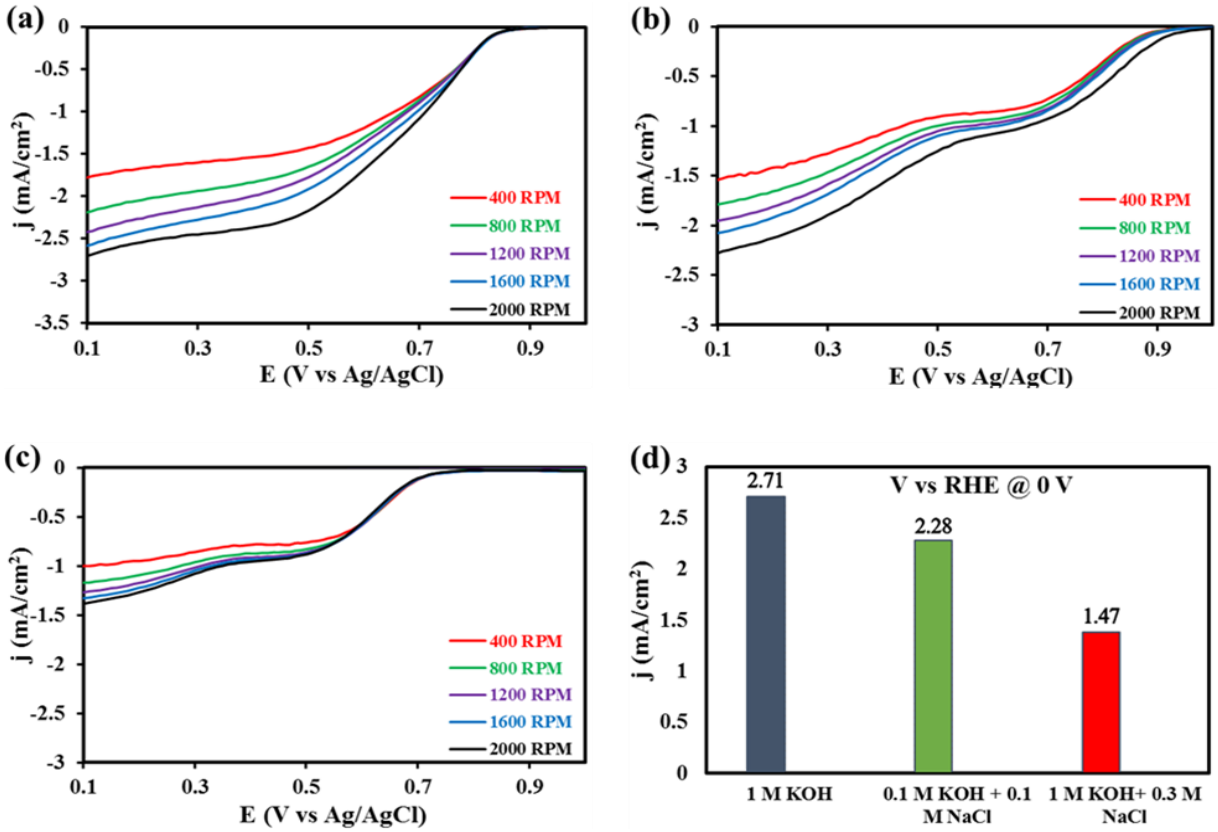

Figure 8. LSV plots of the as-prepared CMT electrocatalyst at RRDE electrodes with different rotation speed at potential scan rate of 10 mV s^{-1} and (**a**) 1 M KOH, (**b**) 1 M KOH + 0.1 M NaCl, and (**c**) 1 M KOH + 0.3 M NaCl. (**d**) Reduction current densities in 0.1 V at different electrolytes.

Table 2. Comparison of electrocatalytic parameters for ORR.

Electrolyte Concentration	Onset vs. RHE * (V)	No. of Transferred Electrons	$E_{1/2}$ * (V)	Diffusion Limited Current Density * (mA cm^{-2})
1 M KOH	0.84	3.75	0.75	3.08
1 M KOH+ 0.1 M NaCl	0.88	3.46	0.71	2.62
1 M KOH+ 0.3 M NaCl	0.74	3.31	0.65	1.47

* The data are measured at 2000 RPM.

To obtain a more comprehensive knowledge of the mechanism of ORR on CMT electrocatalyst, Koutecky–Levich (KL) curves were plotted at different potentials for 1 M KOH, 1 M KOH + 0.1 M NaCl, and 0.1 M KOH + 0.3 M NaCl, as shown in Figure 9. The first-order reduction reaction kinetics of the dissolved oxygen, with respect to the concentration of oxygen dissolved in the electrolytes, may be proven from the linear behavior of K–L plots in Figure 9. Furthermore, the parallel nature of the fitted lines of the K–L graphs at different applied potentials indicates first order kinetics towards the concentration of dissolved oxygen and electron transfer pathways of similar nature for ORR [47,48].

The number of electrons transferred (n) during ORR was estimated from Equation (3) as explained above, and it was estimated to be 3.75 in 1 M KOH at a potential range of 0.2–0.35 V, which suggests a four-electron reduction pathway forming water as dominant product for ORR [49,50]. Similarly, the number of electrons transferred in 1 M KOH + 0.3 M NaCl and 1 M KOH + 0.1 M NaCl electrolytes for the same potential range of 0.2–0.35 V was estimated to be 3.46 and 3.31, respectively, suggesting four electron

reduction pathways even in the presence of high salt concentrations in the electrolytes. The fact that oxygen could be completely reduced to water in alkaline solutions with high salt content via a four-electron pathway reemphasizes the superior performance of CoMoTe in ORR which might be due to the presence of the abundant soluble ions in seawater, which can effectively accelerate the charge transfer. The superior performance of CoMoTe for ORR in seawater coupled with its OER and HER activity, confirmed its great potential as a tri-functional electrocatalyst for sustainable energy storage/conversion from naturally occurring seawater.

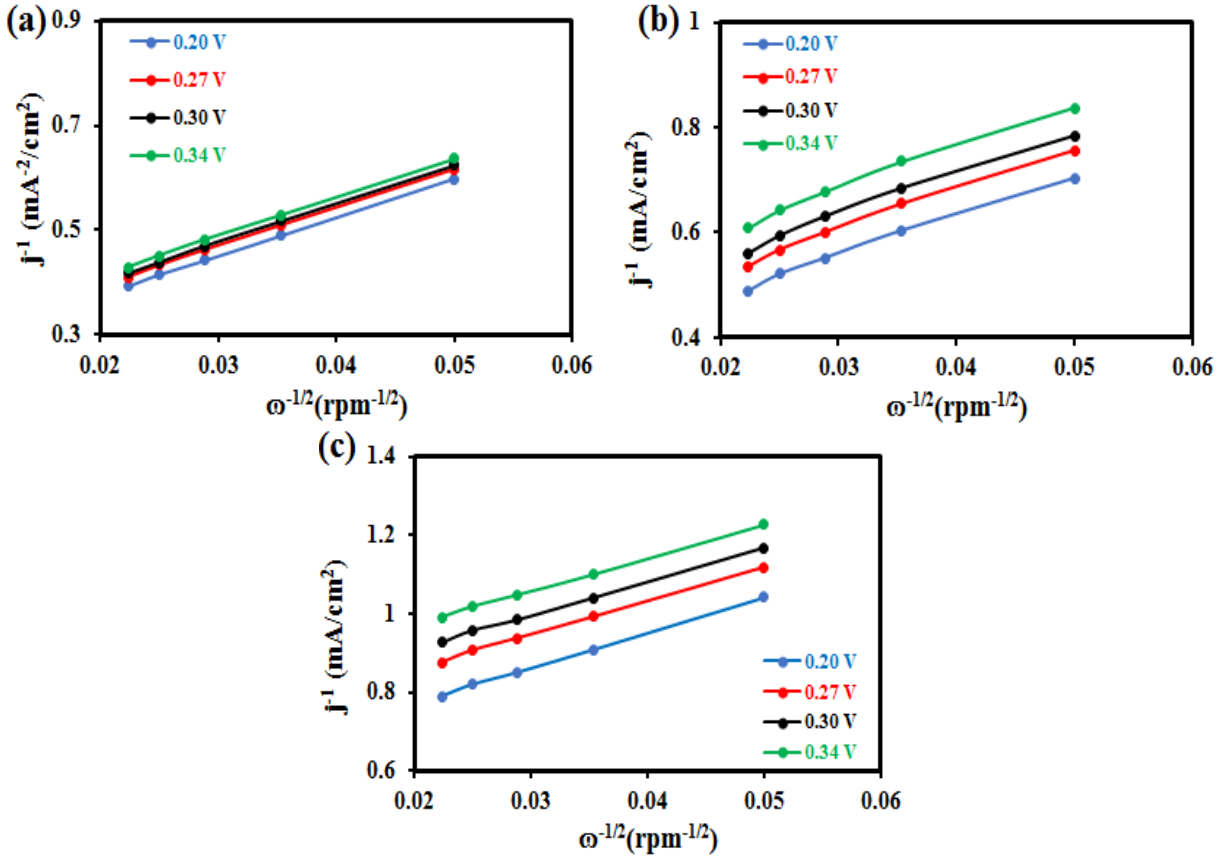

Figure 9. K–L plots of CMT electrode in O_2-saturated (**a**) 1 M KOH, (**b**) 1 M KOH + 0.3 M NaCl solution, and (**c**) 1 M KOH + 0.1 M NaCl, collected using RDE set-up.

3. Experimental

3.1. Materials

All the chemicals that were utilized in the hydrothermal synthesis of CoMoTe were of analytical grade and employed as received. Deionized water (DI) of a resistivity of 18 MΩ cm was utilized for solution preparation. Cobalt nitrate ($Co(NO_3)_2{\cdot}6H_2O$) and molybdenum hexacarbonyl ($Mo(CO)_6$) were obtained from Sigma-Aldrich (St. Louis, MO, USA), while hydrazine hydrate ($N_2H_4{\cdot}H_2O$) of 100% purity and tellurium dioxide (TeO_2) were sourced from Thermo Scientific Chemicals (Waltham, MA, USA). Nafion and the carbon cloth substrate were supplied by Fuel Cells (Danbury, CT, USA).

3.2. Synthesis of Cobalt Molybdenum Telluride

Cobalt molybdenum telluride (CMT) was synthesized via a hydrothermal method. In 5.0 mL of deionized water, $Co(NO_3)_2{\cdot}6H_2O$ (0.015 M) was dissolved and stirred with the assistance of a magnetic stirrer to achieve a homogeneous solution. After 5 min of stirring, $Mo(CO)_6$ (0.015 M) was added, which was subsequently followed by the addition of 2.0 mL of DI water. Continuous stirring was performed on the mixture for another 5 min,

after which TeO_2 (0.03 M) was introduced. Next, 3.0 mL of DI water was added, and the solution was vigorously stirred for 20 more minutes. Then, 2.0 mL of Hydrazine hydrate ($N_2H_4 \cdot H_2O$) was added, and the mixture was put into continuous stirring for an additional 10 min. The prepared solution was poured into a Teflon-lined stainless-steel autoclave, securely sealed, and heated in an oven at 175 °C for 24 h. The solution was cooled to room temperature, after which the black product was washed and centrifuged multiple times with deionized water. Additional washes were performed with a mixture of deionized water and ethanol to ensure the removal of impurities. The final step involved drying the product in a vacuum oven at 60 °C for 24 h.

3.3. Materials Characterization

Powder X-ray diffraction (PXRD): The crystallinity of the synthesized CMT powder was analyzed using the PXRD, obtained with a Philips X'Pert Powder X-ray diffractometer equipped with Cu–Kα radiation at a wavelength of 1.5406 Å.

Scanning electron microscopy (SEM): The morphology of the hydrothermally prepared sample was examined using SEM images obtained from a scanning electron microscope (FEI Helios NanoLab 600 FIB/FESEM, Thermo Fisher Scientific, USA) at an accelerating voltage of 10 kV and a working distance of 4.5 mm.

X-ray photoelectron spectroscopy (XPS): The chemical composition of the synthesized sample was analyzed through X-ray photoelectron spectroscopy (XPS), utilizing a Kratos Axis 165 X-ray photoelectron spectrometer supplied by Kratos Analytical Limited, situated in Manchester, United Kingdom. With the intention of examining the true surface chemistry, all XPS data were acquired without sputtering.

3.4. Electrochemical Characterization

The electrocatalytic performance of the synthesized CMT electrodes for HER, OER, and ORR was assessed using an IviumStat potentiostat. Electrochemical measurements were performed in a conventional three-electrode system, employing an Ag | AgCl reference electrode (KCl-saturated) the reference electrode and a graphite rod as the counter electrode, while CMT dropcasted on carbon cloth acted as the working electrode. To prepare the working electrode, 5.0 mg of CMT electrocatalyst powder was added in a mixture of 10 µL of Nafion and 300 µL of ethanol. This mixture was ultrasonicated for 30 min to reach a uniform suspension. A total of 100 µL of the resulting suspension was drop-cast onto a CC electrode with a confined surface area of 0.08 cm^2, applied in 10 µL intervals. The film that was dropcasted was left to dry at room temperature overnight and subsequently heated in an oven at 65 °C for an additional 30 min.

The electrochemical data were collected in three different types of electrolyte solutions; (i) 1 M KOH, (ii) 1 M KOH + 0.1 M NaCl (as artificially simulated seawater with moderate salt concentration), and (iii) 1 M KOH + 0.3 M NaCl (as artificially simulated seawater of higher salt concentration). All acquired potentials were referenced against Ag | AgCl and were subsequently converted to the reversible hydrogen electrode (RHE) using the following equation: (Equation (1)) [51]:

$$E_{RHE} = E_{Ag\,|\,AgCl} + 0.059\ pH + E^0{}_{Ag\,|\,AgCl} \quad (1)$$

In this equation, E_{RHE} represents the converted potential vs. RHE, $E_{Ag\,|\,AgCl}$ is the experimentally applied potential, and $E^0{}_{Ag\,|\,AgCl}$ denotes the standard potential of Ag | AgCl electrode at 25 °C, which is 0.199 V.

ORR kinetics were studied using a rotating disc electrode (RDE) in an oxygen-saturated electrolyte, with electrode rotation rates ranging between 400 and 2000 rpm, increasing in 400 rpm increments. The total number of electrons transferred during the ORR reaction was estimated using a Koutecky–Levich (K-L) plot that was constructed (J^{-1} vs. $\omega^{-1/2}$) using the K–L equation (Equation (2)) [52]:

$$1/J = 1/(B\omega^{1/2}) + 1/J_K \quad (2)$$

Here, J is the recorded current density (A cm^{-2}), J_K is kinetic current density, and ω denotes angular rotation rate of the electrode (rad/s). B is called the Levich constant, which is usually calculated from the slope of K–L plots based on the Equation (3) [53]:

$$B = 0.2nFC_0 (D_0)^{2/3} \nu^{-1/6} \quad (3)$$

In Equation (3), n is defined as the number of electrons exchanged per molecule of O_2, F represents the Faraday constant (96,485 C mol^{-1}), C_0 denotes the amount of oxygen concentration in the bulk of the electrolyte (1.2×10^{-6} mol cm^{-3}), D_0 is the diffusion coefficient of O_2 (1.9×10^{-5} cm^2 s^{-1}), and ν is the kinematic viscosity of the electrolyte (0.01 cm^2 s^{-1}).

The electrokinetic properties of the CMT electrocatalyst in OER reaction was examined by Tafel slope, which was calculated from the Tafel plot driving from the Tafel equation (Equation (4)) [54].

$$\eta = a + \frac{2.3RT}{\alpha nF} log\ j \quad (4)$$

where α indicates the transfer coefficient, n is the number of electrons participating in the reaction, F represents the Faraday constant, j is the current density, and η stands for overpotential of oxygen evolution reaction, calculated by $\eta = E - E_r$, where E represents the applied potential, while E_r denotes the thermodynamic water splitting voltage, i.e., 1.23 V. In Equation (4), the Tafel slope is expressed as 2.3 $RT/\alpha nF$. The smaller the Tafel slope, the faster the reaction kinetic at the catalyst's surface is [55].

3.5. Gas-Phase Product Identification from OER

The gas products of OER reaction have been analyzed using a gas chromatograph (GC). The gas chromatograph instrument was equipped with a thermal conductivity detector (GC-TCD) and Molecular Sieve 5A capillary column with the carrier gas of helium (99.999%). For GC analysis, the OER reaction was conducted in a closed cell using CMT electrocatalyst, and the evolved gas from the reaction at the anode was collected after the chronoamperometry experiment to be injected into the GC-TCD equipment at variable reaction times using a gas-tight syringe. The respective chromatograph was compared to the corresponding results obtained by the injection of pure chlorine, oxygen, and nitrogen gases.

4. Conclusions

In the current study, cobalt molybdenum telluride was investigated as a promising tri-functional electrocatalyst for HER, OER, and ORR reactions in alkaline seawater. The electrocatalyst was synthesized through a hydrothermal route and the physicochemical properties were characterized with several techniques. Detailed electrochemical analysis showed that CoMoTe has a superior activity for OER and HER reactions in alkaline seawater with high salt concentration, as evident through the high current density and low overpotentials. It also exhibits high operational and compositional stability for a prolonged time. More importantly, as the OER overpotential was reduced, no chlorine was detected even after long-term operation, suggesting that the catalyst interface was not much affected by the presence of the saline content in seawater and selectively oxidized water. It was also observed that although increased concentrations of cations like sodium (Na^+) in seawater may compete with hydrogen ions (H^+) for adsorption sites on the electrode surface in HER, the CoMoTe electrocatalyst could retain its HER activity to a high extent even at higher NaCl concentrations. Thus, this research reports a new electrocatalyst composition, which is a first of its kind to exhibit significant performance for clean energy production/storage from alkaline seawater.

Author Contributions: Methodology, R.K.; Validation, A.N. and H.S.; Formal analysis, R.K. and A.N.; Investigation, R.K.; Writing—original draft, R.K. and A.N.; Writing—review & editing, M.N.; Supervision, M.N.; Project administration, M.N.; Funding acquisition, M.N. All authors have read and agreed to the published version of the manuscript.

Funding: This work was funded through National Science Foundation, (CHE-215175).

Data Availability Statement: Data are contained within the article.

Acknowledgments: The authors would also like to acknowledge Materials Research Center at Missouri S&T for equipment usage.

Conflicts of Interest: The authors declare no conflict of interest.

References

1. Xu, X.; Sun, H.; Jiang, S.P.; Shao, Z. Modulating metal–organic frameworks for catalyzing acidic oxygen evolution for proton exchange membrane water electrolysis. *SusMat* **2021**, *1*, 460–481. [CrossRef]
2. Hu, L.; Tan, X.; Zhang, K. Electrolysis of Direct Seawater: Challenges, Strategies, and Future Prospects. *Chin. J. Chem.* **2023**, *41*, 3484–3492. [CrossRef]
3. Wang, H.-F.; Chen, L.; Pang, H.; Kaskel, S.; Xu, Q. MOF-derived electrocatalysts for oxygen reduction, oxygen evolution and hydrogen evolution reactions. *Chem. Soc. Rev.* **2020**, *49*, 1414–1448. [CrossRef]
4. Tahir, M.; Pan, L.; Idrees, F.; Zhang, X.; Wang, L.; Zou, J.-J.; Wang, Z.L. Electrocatalytic oxygen evolution reaction for energy conversion and storage: A comprehensive review. *Nano Energy* **2017**, *37*, 136–157. [CrossRef]
5. Dresp, S.; Dionigi, F.; Klingenhof, M.; Strasser, P. Direct Electrolytic Splitting of Seawater: Opportunities and Challenges. *ACS Energy Lett.* **2019**, *4*, 933–942. [CrossRef]
6. Gebremariam, G.K.; Jovanović, A.; Pašti, I.A. The Effect of Electrolytes on the Kinetics of the Hydrogen Evolution Reaction. *Hydrogen* **2023**, *4*, 776–806. [CrossRef]
7. Zhang, X.; Xiao, Y.; Tian, G.; Yang, X.; Dong, Y.; Zhang, F.; Yang, X. Enhancing Resistance to Chloride Corrosion by Controlling the Morphologies of PtNi Electrocatalysts for Alkaline Seawater Hydrogen Evolution. *Chemistry* **2022**, *29*, e202202811. [CrossRef]
8. Becker, H.; Murawski, J.; Shinde, D.V.; Stephens, I.E.L.; Hinds, G.; Smith, G. Impact of impurities on water electrolysis: A review. *Sustain. Energy Fuels* **2023**, *7*, 1565–1603. [CrossRef]
9. Kafle, A.; Gupta, D.; Mehta, S.; Garg, K.; Nagaiah, T.C. Recent advances in energy-efficient chlorine production via HCl electrolysis. *J. Mater. Chem. A* **2024**, *12*, 5626–5641. [CrossRef]
10. Maljusch, A.; Nagaiah, T.C.; Schwamborn, S.; Bron, M.; Schuhmann, W. Pt-Ag catalysts as cathode material for oxygen-depolarized electrodes in hydrochloric acid electrolysis. *Anal. Chem.* **2010**, *82*, 1890–1896. [CrossRef]
11. Garg, K.; Kumar, M.; Kaur, S.; Nagaiah, T.C. Electrochemical Production of Hydrogen from Hydrogen Sulfide Using Cobalt Cadmium Sulfide. *ACS Appl. Mater. Interfaces* **2023**, *15*, 27845–27852. [CrossRef] [PubMed]
12. Li, J.; Jia, Q.; Ghoshal, S.; Liang, W.; Mukerjee, S. Highly Active and Stable Fe–N–C Catalyst for Oxygen Depolarized Cathode Applications. *Langmuir* **2017**, *33*, 9246–9253. [CrossRef] [PubMed]
13. Wang, H.-Y.; Weng, C.-C.; Ren, J.-T.; Yuan, Z.-Y. An overview and recent advances in electrocatalysts for direct seawater splitting. *Front. Chem. Sci. Eng.* **2021**, *15*, 1408–1426. [CrossRef]
14. Zhang, W.; Cui, L.; Liu, J. Recent advances in cobalt-based electrocatalysts for hydrogen and oxygen evolution reactions. *J. Alloys Compd.* **2020**, *821*, 153542. [CrossRef]
15. Liu, J.; Duan, S.; Shi, H.; Wang, T.; Yang, X.; Huang, Y.; Wu, G.; Li, Q. Rationally Designing Efficient Electrocatalysts for Direct Seawater Splitting: Challenges, Achievements, and Promises. *Angew. Chem.* **2022**, *61*, e202210753. [CrossRef]
16. Li, C.; Baek, J.-B. Recent Advances in Noble Metal (Pt, Ru, and Ir)-Based Electrocatalysts for Efficient Hydrogen Evolution Reaction. *ACS Omega* **2019**, *5*, 31–40. [CrossRef]
17. Udayakumar, A.; Dhandapani, P.; Ramasamy, S.; Yan, C.; Angaiah, S. Recent developments in noble metal–based hybrid electrocatalysts for overall water splitting. *Ionics* **2023**, *30*, 61–84. [CrossRef]
18. Pan, S.; Ma, Z.; Yang, W.; Dongyang, B.; Yang, H.; Lai, S.; Dong, F.; Yang, X.; Lin, Z. Magnesium incorporation activates perovskite cobaltites toward efficient and stable electrocatalytic oxygen evolution. *Mater. Rep. Energy* **2023**, *3*, 100212. [CrossRef]
19. Qian, Y.; Khan, I.A.; Zhao, D. Electrocatalysts Derived from Metal-Organic Frameworks for Oxygen Reduction and Evolution Reactions in Aqueous Media. *Small* **2017**, *13*, 1701143. [CrossRef]
20. Majhi, K.C.; Yadav, M. Transition Metal-Based Chalcogenides as Electrocatalysts for Overall Water Splitting. *ACS Eng. Au* **2023**, *3*, 278–284. [CrossRef]
21. Huang, Y.; Jiang, L.; Shi, B.; Ryan, K.M.; Wang, J. Highly efficient oxygen evolution reaction enabled by phosphorus doping of the FE electronic structure in iron–nickel selenide nanosheets. *Adv. Sci.* **2021**, *8*, 2101775. [CrossRef] [PubMed]
22. Yin, Z.-H.; Huang, Y.; Song, K.; Li, T.-T.; Cui, J.-Y.; Meng, C.; Zhang, H.; Wang, J.-J. Ir Single Atoms Boost Metal–Oxygen Covalency on Selenide-Derived NiOOH for Direct Intramolecular Oxygen Coupling. *J. Am. Chem. Soc.* **2024**, *146*, 6846–6855. [CrossRef] [PubMed]
23. Liu, X.; Chi, J.; Mao, H.; Wang, L. Principles of Designing Electrocatalyst to Boost Reactivity for Seawater Splitting. *Adv. Energy Mater.* **2023**, *13*, 2301438. [CrossRef]
24. Wu, Z.; Lu, X.F.; Zang, S.; Lou, X.W. Non-Noble-Metal-Based Electrocatalysts toward the Oxygen Evolution Highly Efficient Oxygen Evolution Reaction Enabled byPhosphorus Doping of theReaction. *Adv. Funct. Mater.* **2020**, *30*, 1910274. [CrossRef]

25. Zhang, Y.; Guo, Z. Transition metal compounds: From properties, applications to wettability regulation. *Adv. Colloid Interface Sci.* **2023**, *321*, 103027. [CrossRef]
26. Lei, Y.; Miao, N.; Zhou, J.; Hassan, Q.U.; Wang, J. Novel magnetic properties of CoTe nanorods and diversified CoTe2 nanostructures obtained at different NaOH concentrations. *Sci. Technol. Adv. Mater.* **2017**, *18*, 325–333. [CrossRef]
27. Wiberg, H.; Johann, K.; Arenz, M. Investigation of the Oxygen Reduction Activity on Silver—A Rotating Disc Electrode Study. *Fuel Cells* **2010**, *10*, 575–581. [CrossRef]
28. Anantharaj, S.; Noda, S. How properly are we interpreting the Tafel lines in energy conversion electrocatalysis? *Mater. Today Energy* **2022**, *29*, 101123. [CrossRef]
29. Razaq, R.; Sun, D.; Xin, Y.; Li, Q.; Huang, T.; Zhang, Z.; Huang, Y. Nanoparticle Assembled Mesoporous MoO_2 Microrods Derived from Metal Organic Framework and Wrapped with Graphene as the Sulfur Host for Long-Life Lithium-Sulfur Batteries. *Adv. Mater. Interfaces* **2018**, *6*, 1801636. [CrossRef]
30. Saxena, A.; Singh, H.; Nath, M. Cobalt telluride electrocatalyst for selective electroreduction of CO_2 to value-added chemicals. *Mater. Renew. Sustain. Energy* **2022**, *11*, 115–129. [CrossRef]
31. Manikandan, M.; Subramani, K.; Sathish, M.; Dhanuskodi, S. Hydrothermal synthesis of cobalt telluride nanorods for a high-performance hybrid asymmetric supercapacitor. *RSC Adv.* **2020**, *10*, 13632–13641. [CrossRef] [PubMed]
32. De Silva, U.; Masud, J.; Zhang, N.; Hong, Y.; Liyanage, W.P.R.; Zaeem, M.A.; Nath, M. Nickel telluride as a bifunctional electrocatalyst for efficient water splitting in alkaline medium. *J. Mater. Chem. A* **2018**, *6*, 7608–7622. [CrossRef]
33. Gao, X.; Wang, Z.; Ashok, J.; Kawi, S. A comprehensive review of anti-coking, anti-poisoning and anti-sintering catalysts for biomass tar reforming reaction. *Chem. Eng. Science. X* **2020**, *7*, 100065. [CrossRef]
34. Khan, M.A.; Zhao, H.; Zou, W.; Chen, Z.; Cao, W.; Fang, J.; Xu, J.; Zhang, L.; Zhang, J. Recent Progresses in Electrocatalysts for Water Electrolysis. *Electrochem. Energy Rev.* **2018**, *1*, 483–530. [CrossRef]
35. Sun, F.; Qin, J.; Wang, Z.; Yu, M.; Wu, X.; Sun, X.; Qiu, J. Energy-saving hydrogen production by chlorine-free hybrid seawater splitting coupling hydrazine degradation. *Nat. Commun.* **2021**, *12*, 4182. [CrossRef]
36. Mefford, J.T.; Zhao, Z.; Bajdich, M.; Chueh, W.C. Interpreting Tafel behavior of consecutive electrochemical reactions through combined thermodynamic and steady state microkinetic approaches. *Energy Environ. Sci.* **2020**, *13*, 622–634. [CrossRef]
37. Kang, X.; Yang, F.; Zhang, Z.; Liu, H.; Ge, S.; Hu, S.; Li, S.; Luo, Y.; Yu, Q.; Liu, Z.; et al. A corrosion-resistant RuMoNi catalyst for efficient and long-lasting seawater oxidation and anion exchange membrane electrolyzer. *Nat. Commun.* **2023**, *14*, 3607. [CrossRef]
38. Liu, G.; Xu, Y.; Yang, T.; Jiang, L. Recent advances in electrocatalysts for seawater splitting. *Nano Mater. Sci.* **2023**, *5*, 101–116. [CrossRef]
39. Zhuang, L.; Li, S.; Li, J.; Wang, K.; Guan, Z.; Liang, C.; Xu, Z. Recent Advances on Hydrogen Evolution and Oxygen Evolution Catalysts for Direct Seawater Splitting. *Coatings* **2022**, *12*, 659. [CrossRef]
40. Jin, H.; Wang, X.; Tang, C.; Vasileff, A.; Li, L.; Slattery, A.; Qiao, S. Stable and Highly Efficient Hydrogen Evolution from Seawater Enabled by an Unsaturated Nickel Surface Nitride. *Adv. Mater.* **2021**, *33*, 2007508. [CrossRef]
41. Marimuthu, T.; Yuvakkumar, R.; Ravi, G.; Xu, X.; Xu, G.; Velauthapillai, D. Hydrothermal construction of flower-like CuS microsphere electrocatalysts for hydrogen evolution reactions in alkaline fresh water, alkaline seawater, and seawater. *Int. J. Energy Res.* **2022**, *46*, 19723–19736. [CrossRef]
42. Nath, M.; De Silva, U.; Singh, H.; Perkins, M.; Wipula, P.R.L.; Umapathi, S.; Chakravarty, S.; Masud, J. Cobalt Telluride: A Highly Efficient Trifunctional Electrocatalyst for Water Splitting and Oxygen Reduction. *ACS Appl. Energy Mater.* **2021**, *4*, 8158–8174. [CrossRef]
43. Zhao, Q.; Wang, Y.; Xiao, F.W.H.L.; Lyu, Y.; Liao, C.; Shao, M. Approaching a high-rate and sustainable production of hydrogen peroxide: Oxygen reduction on Co–N–C single-atom electrocatalysts in simulated seawater. *Energy Environ. Sci.* **2021**, *14*, 5444–5456. [CrossRef]
44. Zhao, Z.; Shen, P.K. Mechanism of Oxygen Reduction Reaction. In *Electrochemical Oxygen Reduction*; Shen, P.K., Ed.; Springer: Singapore, 2021.
45. Zhan, Y.; Ding, Z.-B.; He, F.; Lv, X.; Wu, W.-F.; Lei, B.; Liu, Y.; Yan, X. Active site switching of Fe-N-C as a chloride-poisoning resistant catalyst for efficient oxygen reduction in seawater-based electrolyte. *Chem. Eng. J.* **2022**, *443*, 136456. [CrossRef]
46. Tylus, U.; Jia, Q.; Hafiz, H.; Allen, R.J.; Barbiellini, B.; Bansil, A.; Mukerjee, S. Engendering anion immunity in oxygen consuming cathodes based on Fe-N-x electrocatalysts: Spectroscopic and electrochemical advanced characterizations. *Appl. Catal. B Environ.* **2016**, *198*, 318–324. [CrossRef]
47. Mukherjee, M.; Samanta, M.; Banerjee, P.; Chattopadhyay, K.K.; Das, G.P. Endorsement of Manganese Phthalocyanine microstructures as electrocatalyst in ORR: Experimental and computational study. *Electrochim. Acta* **2019**, *296*, 528–534. [CrossRef]
48. Liang, Y.; Li, Y.; Wang, H.; Zhou, J.; Wang, J.; Regier, T.; Dai, H. Co3O4 nanocrystals on graphene as a synergistic catalyst for oxygen reduction reaction. *Nat. Mater.* **2011**, *10*, 780–786. [CrossRef]
49. Yin, M.; Miao, H.; Hu, R.; Sun, Z.; Li, H. Manganese dioxides for oxygen electrocatalysis in energy conversion and storage systems over full pH range. *J. Power Sources* **2021**, *494*, 229779. [CrossRef]
50. Wang, X.; Li, Z.; Qu, Y.; Yuan, T.; Wang, W.; Wu, Y.; Li, Y. Review of Metal Catalysts for Oxygen Reduction Reaction: From Nanoscale Engineering to Atomic Design. *Chem* **2019**, *5*, 1486–1511. [CrossRef]
51. Nath, M.; Singh, H.; Saxena, A. Progress of transition metal chalcogenides as efficient electrocatalysts for energy conversion. *Curr. Opin. Electrochem.* **2022**, *34*, 100993. [CrossRef]

52. Chen, H.; Liu, Y.; Liu, B.; Yang, M.; Li, H.; Chen, H. Hypercrosslinked polymer-mediated fabrication of binary metal phosphide decorated spherical carbon as an efficient and durable bifunctional electrocatalyst for rechargeable Zn–air batteries. *Nanoscale* **2022**, *14*, 12431–12436. [CrossRef] [PubMed]
53. Li, J.; Chen, M.; Cullen, D.A.; Hwang, S.; Wang, M.; Li, B.; Liu, K.; Karakalos, S.; Lucero, M.; Zhang, H.; et al. Atomically dispersed manganese catalysts for oxygen reduction in proton-exchange membrane fuel cells. *Nat. Catal.* **2018**, *1*, 935–945. [CrossRef]
54. Abdullahi, I.M.; Nath, M. Molecular Cluster Complex of High-Valence Chromium Selenide Carbonyl as Effective Electrocatalyst for Water Oxidation. *Catalysts* **2023**, *13*, 721. [CrossRef]
55. Wang, L.; Lee, C.-Y.; Schmuki, P. Solar water splitting: Preserving the beneficial small feature size in porous α-Fe2O3photoelectrodes during annealing. *J. Mater. Chem. A* **2013**, *1*, 212–215. [CrossRef]